Quantum magnetic interactions in $\boldsymbol{S} = 1/2$ $KCuCl_3$

2000 J. Phys.: Condens. Matter 12 5463

(http://iopscience.iop.org/0953-8984/12/25/310)

J. Phys.: Condens. Matter **12** (2000) 5463–5472. Printed in the UK PII: S0953-8984(00)11912-5

Quantum magnetic interactions in $S = 1/2$ $KCuCl_3$

N Cavadini†, G Heigold†, W Henggeler†, A Furrer†, H-U Güdel‡, K Krämer‡ and H Mutka§

† Laboratory for Neutron Scattering, ETH Zürich & Paul Scherrer Institut, CH-5232 Villigen PSI, Switzerland

‡ Department for Chemistry and Biochemistry, Universität Bern, CH-3000 Bern 9, Switzerland

§ Institut Laue–Langevin, BP 156, F-38042 Grenoble Cédex 9, France

E-mail: nordal.cavadini@psi.ch

Received 16 February 2000

Abstract. $KCuCl_3$ is an $S = 1/2$ magnetic insulator with a singlet ground state and a finite spin excitation gap. Above the gap, dispersive triplet excitation modes propagate in the whole reciprocal space. From single-crystal inelastic neutron investigations the three-dimensional coupling scheme is rationalized in the framework of a dimer Heisenberg model, and related to the structural features of $KCuCl_3$. The experimental and theoretical characterization presented completes earlier works on the compound under investigation, providing also higher-order expressions for the singlet–triplet dispersion relation. The latter may also be of relevance for the parent quantum systems $TlCuCl_3$ and NH_4CuCl_3, albeit at different coupling ratios with respect to $KCuCl_3$.

1. Introduction

Low-dimensional $S = 1/2$ antiferromagnets are unconventional spin systems dominated by quantum fluctuations. Usual model approaches—like spin-wave theory based on a staggered Néel ground state—prove to be inadequate to describe the behaviour of intrinsically quantum disordered magnetic insulators. However, in the case where the coupling scheme features a strong imbalance in the exchange constants, the essential magnetic properties can be captured by a dimer model [1]. This approach considers the dominant antiferromagnetic (AF) pair correlation exactly, naturally providing a singlet nonmagnetic ground state and gapped singlet–triplet excitations. Both properties are common to several $S = 1/2$ quantum systems, like alternating chains, even-leg ladders and dimer compounds in general. The additional weak interdimer interactions distinctive of each given system are considered perturbatively in the dimer model,

$$H = \underbrace{-J \sum_{\langle i \rangle} S_{i1} S_{i2}}_{H^{(0)}} \underbrace{- \sum_{\langle ij,\mu\nu \rangle} J_{ij,\mu\nu} S_{i\mu} S_{j\nu}}_{H^{(1)}} \tag{1}$$

where $H^{(0)}$ accounts for the isolated dimers, and $H^{(1)}$ considers interactions between neighbouring dimers $\langle ij \rangle$, generally mediated by the spins $\mu = \{1, 2\}$, $\nu = \{1, 2\}$ at sites i and j, respectively. At first order, $H^{(1)}$ yields Bloch-like triplet waves which can propagate from dimer i to dimer j according to the specific coupling scheme. Their energy shows weak dispersive behaviour across the localized limit $|J|$, with the absolute minimum determining the gap. From an experimental point of view, static measurements (χ, M) and local probes

0953-8984/00/255463+10$30.00

(NMR, EPR) can monitor the gap accurately but are less conclusive in the determination of the complete excitation spectrum. This information is nevertheless essential to clarify the nature of such unconventional spin systems, as exemplified for the $S = 1/2$ AF compound $(VO)_2P_2O_7$, which was originally proposed to be a realization of a two-leg ladder but turned out to be an alternating-chain compound after comprehensive neutron investigations [2].

The requirement of direct and complete access to both time and space spin–spin correlations promotes inelastic neutron scattering (INS) as the definitive technique to characterize magnetic systems in general, and spin-gap compounds in particular. In this contribution, INS results for high-quality single crystals of $KCuCl_3$ are rationalized in the context of a dimer Heisenberg model, and related to the structural properties of the specific system under investigation. The paper is organized as follows. In section 2 the interplay between the crystal structure of $KCuCl_3$ and the magnetic interactions among the Cu^{2+} ions in the unit cell is presented; in section 3 detailed model expectations are developed in accordance with the proposed exchange coupling scheme. Analytical expressions for the spin–spin correlation function $S(\kappa, \omega)$ are presented. The theoretical discussion is supported in section 4 by conclusive INS measurements, which confirm the validity of the microscopic model approach completing at the same time the experimental picture of $KCuCl_3$. As an improvement to previous neutron investigations, all measurements have been performed on high-resolution spectrometers, allowing accurate quantitative determination of the model parameters. Second-order corrections for the energy dispersion of the excitations are presented in a strong-coupling expansion for the first time, and successfully applied in the data evaluation.

2. Structure

Monoclinic $KCuCl_3$ crystallizes in the $P2_1/c$ space group, with lattice constants $a = 4.029$ Å, $b = 13.785$ Å, $c = 8.736$ Å, and $\beta = 97.20^\circ$ [3]. The structure consists of double chains of edge-sharing $CuCl_6$ complexes, which run parallel to the short axis a, occupy the edges and the centre of the bc-plane and are separated from each other by K^+ cations (figure 1). The Cu coordination is of the distorted octahedral type common to the Jahn–Teller Cu^{2+} cation, resulting in complete orbital momentum quenching. Well localized spins $S = 1/2$ are expected to reside at the Cu site in a $3d_{x^2-y^2}$ configuration whose lobes point to the vertices of a fourfold, nearly planar Cl environment corresponding to the base of the distorted octahedra. Magnetic interaction between the Cu^{2+} is provided in a first approximation by superexchange pathways through the 3p and 3s orbitals of the Cl^- anions [4]. Appreciable exchange coupling within the double chains may be expected between neighbouring Cu which share common bridging Cl, building nearly planar $(Cu_2Cl_6)^{2-}$ dimer clusters—a structure often assumed by Cu^{2+} pairs [5]. Due to the octahedral distortion, additional intrachain interactions perpendicular to the dimer planes are not likely to play a major role. The same holds for eventual interchain interactions, which involve at least two anion pathways Cu–Cl–Cl–Cu and may thus be expected to provide smaller couplings with respect to the Cu–Cl–Cu dimer exchange. In the light of the above considerations, the magnetic properties of $KCuCl_3$ are possibly captured by an $S = 1/2$ Heisenberg model consisting of dimers weakly interacting together, as first suggested in [6] and rationalized in [7]. Since the compound shows a singlet ground state, an AF intradimer coupling has been proposed [6, 8]. Whereas a square-planar coordination featuring 90° bonds through orthogonal 3p orbitals would be weakly ferromagnetic (see [9] for the Cu–O–Cu case), slight distortions towards linear bondings are known to increase the importance of the AF exchange term according to the Goodenough and Kanamori rules. The $\sim 96^\circ$ bond angle of the nearly planar $(Cu_2Cl_6)^{2-}$ dimer is assumed to be in this limit, providing AF intradimer exchange $J < 0$. An inspection of additional pathways within the double chains indicates the possibility

Table 1. Microscopic contributions to the effective exchange constants J_{ij} in $KCuCl_3$; cf. figure 1. Suggested couplings between dimers i and j are listed as three-ion and four-ion pathways A–B–C (–D), following the criteria and the notation explained in the text. Bond distances R (Å) and bond angles $\angle$ (deg) are derived from [3] in the form $|R_{AB}|$–$\angle_{ABC}$–$|R_{BC}|$ (–$\angle_{BCD}$–$|R_{CD}|$).

J_{ij}	R_{ij} (l.u.)	$J_{ij,\mu\nu}$	Pathways, distances and angles
J_a	(1 0 0)	$J_{ij,11}$	Cu{i, 1}–Cl_2{i}–Cu{j, 1} ··· –Cl_3{j}– ···
			2.267–100.6–2.941 3.113–94.5–2.323
		$J_{ij,22}$	Cu{i, 2}–Cl_2{i}–Cu{j, 2} ··· –Cl_3{j}– ···
			2.941–100.6–2.267 2.323–94.5–3.113
		$J_{ij,12}$	Cu{i, 1}–Cl_3{i}–Cu{j, 2} ··· –Cl_3{j}– ···
			2.314–90.9–3.113 3.113–90.9–2.314
J_{a2c}	(2 0 1)	$J_{ij,12}$	Cu{i, 1}–Cl_2{i}–Cl_2{j}–Cu{j, 2}
			2.267–153.5–3.796–153.5–2.267
J_{abc}	(1 1/2 1/2)	$J_{ij,22}$	Cu{i, 2}–Cl_3{i}–Cl_1{j}–Cu{j, 2}
			2.322–149.9–3.843–148.7–2.248
	(1 $\bar{1}$/2 1/2)	$J_{ij,11}$	Cu{i, 1}–Cl_1{i}–Cl_3{j}–Cu{j, 1}
			2.248–148.7–3.843–149.9–2.322
J	(0 0 0)	$J_{ij,12}$	Cu{i, 1}–Cl_3{i}–Cu{i, 2} ··· –Cl_3{i}– ···
			2.322–95.9–2.314 2.314–95.9–2.322

of weak interdimer exchange J_a along $\pm(1, 0, 0)$ lattice units (l.u.), involving the elongated apical distances of the octahedra rather than the short basal distances. Suggested Cu–Cl–Cu correlations on the length scale of the axis a are reported in table 1, in a notation corresponding to the model approach of section 3. Regarding exchange between different double chains, the terminal chlorines within the dimers may provide weak Cu–Cl–Cl–Cu pathways. These would require rather direct overlap with bonding angles preferentially near to 180° and directions possibly following the dimer planes. The Cu–Cl–Cl–Cu exchange paths featuring bonding angles bigger than 148° over distances on the scale of a are listed in table 1. They provide qualitative support for a J_{a2c}-interaction which would couple dimers along $\pm(2, 0, 1)$ l.u. within the same sublattice. Also, they suggest a star-like coupling J_{abc} between edge dimers and centre dimers, following the pathways $\pm(1, 1/2, 1/2)$ and $\pm(1, -1/2, 1/2)$. Both the proposed J_{a2c}- and J_{abc}-couplings are perpendicular to the $(1, 0, -2)$ direction, which in turn is nearly normal to the dimer planes (figure 1). Other superexchange paths for either interchain or intrachain couplings were found to involve less favourable configurations with respect to the criteria expressed above. As will be demonstrated according to the experimental results in section 4, the exchange interactions described lead to the effective dimer coupling scheme which correctly accounts for the experimental observations. The resulting model parameters, to be formalized in section 3, are in accordance with the relevant couplings presented in [7] after INS investigations along the crystallographic directions $\boldsymbol{a}^*$, $\boldsymbol{b}^*$, and $\boldsymbol{c}^*$. In a recent work, similar conclusions were proposed based on measurements in the a^*c^*-plane [10]. Improving on previous studies on $KCuCl_3$, we conclusively support at leading order not only the validity but also the completeness of the effective three-dimensional couplings resulting from the above dimer approach.

3. Excitations

Expectations for the energy dependence of the singlet–triplet excitations can be readily obtained from a strong-coupling expansion applied to the unperturbed dimer basis; see [11, 12] for

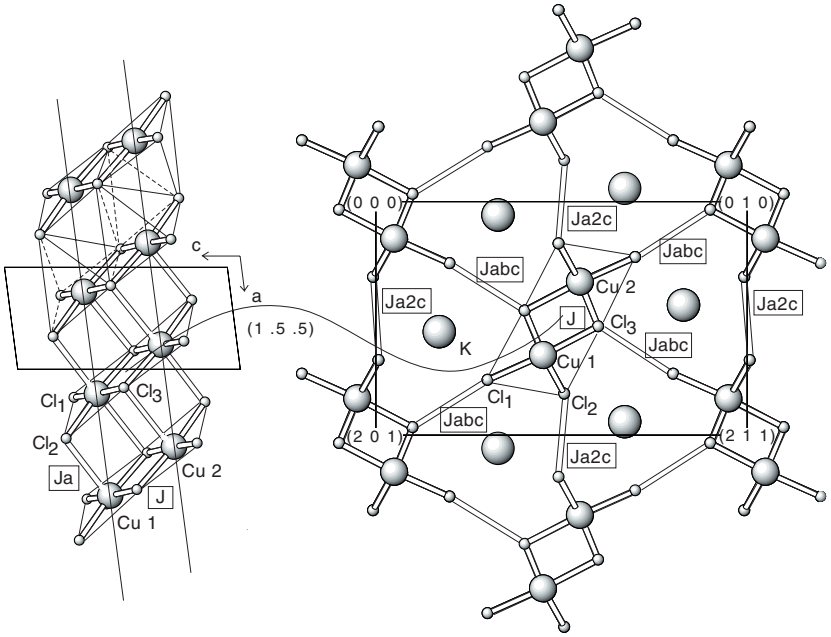

Figure 1. A schematic view of the structure and the magnetic interaction paths in $KCuCl_3$; cf. table 1. Left: $(Cu_2Cl_6)^{2-}$ dimers are located in the basal planes of distorted, edge-sharing octahedra. These are stacked in double chains along the a-direction. Right: the double chains occupy the edges and the centre of the bc-plane. Magnetic interactions J, J_{a2c}, J_{abc} (in the plane) and J_a (out of the plane) determined by the tilted dimer arrangement in the unit cell are accordingly highlighted.

recent examples. The energy scale is provided by $H^{(0)}$ from equation (1), yielding localized $S = 0 \rightarrow S = 1$ dimer transitions at

$$\epsilon^{(0)} = -J \qquad J < 0. \tag{2}$$

First-order corrections $H^{(1)}$ introduce a dispersion which corresponds to the Fourier transform of the additional weak couplings between the dimers:

$$\epsilon_{\pm}^{(1)}(q) = -\{J_a \cos(2\pi q_h) + J_{a2c} \cos(4\pi q_h + 2\pi q_l) \pm 2J_{abc} \cos(\pi q_k) \cos(2\pi q_h + \pi q_l)\} \tag{3}$$

where the wavevector $q = (q_h, q_k, q_l)$ is expressed in reciprocal-lattice units (r.l.u.), and J_{ij} are the effective exchange constants introduced in section 2. The periodicity of the dispersion relation is indicative of the interdimer couplings involved, the amplitude depends on the nature and strength of the respective exchange constants. Two excitation branches $\epsilon_{\pm}(q) = \epsilon^{(0)} + \epsilon_{\pm}^{(1)}(q)$ are generally expected in $KCuCl_3$ as required by the presence of two dimers in the chemical unit cell (figure 1). The exclusive singlet–triplet correlation function $S_{\pm}(\kappa, \omega)$ provides at first order expectations for their intensities:

$$S_{\pm}^{\alpha\alpha}(\kappa, \omega) = \left(\frac{1}{2}\sin\left(\kappa\frac{R_1}{2}\right) \pm \frac{1}{2}\sin\left(\kappa\frac{R_2}{2}\right)\right)^2 \left(\frac{\epsilon^{(0)} - \epsilon_{\pm}^{(1)}(q)}{|J|}\right)\delta(\hbar\omega - \epsilon^{(0)} - \epsilon_{\pm}^{(1)}(q)) \tag{4}$$

with $\alpha = \{x, y, z\}$ labelling the spin coordinate, $\kappa = q + \tau$ the scattering wavevector. The expression for $S_{\pm}(\kappa, \omega)$ presented above is fully isotropic in spin space. In equation (1) and in the following analysis, exchange anisotropy is not incorporated. This is justified by the true $S = 1/2$ nature of the magnetic interactions in $KCuCl_3$, and supported by detailed static

experiments [16]. $R_1 = 0.48a + 0.10b + 0.32c$ and $R_2 = 0.48a - 0.10b + 0.32c$ in equation (4) correspond to the intradimer spin separation at the edges and in the centre of the bc-plane, respectively (figure 1). The resulting characteristic intensity envelope in the correlation function has been presented in our previous investigations [7]. It originates from the extended dimer nature of the magnetic excitations—involving two separate spins on each dimer—and implies for the present work that on the a^*c^*-scattering plane (where $\kappa R_1 = \kappa R_2$) only the ϵ_+-branch is visible, whereas on the b^*c^*-scattering plane both ϵ_+ and ϵ_- are generally visible. Accordingly, we will refer to the symmetry a^*c^*-plane, and to the generic b^*c^*-plane.

In the following we concentrate on the energy dependence of the dispersion relation with two aims: first, to confirm the validity of the interdimer coupling scheme corresponding to equation (3) on the basis of additional experimental evidence; second, to present and apply second-order corrections for the singlet–triplet dispersion relation. The first aim results from the observation that our previous measurements were performed parallel to the crystallographic axes, fulfilling a compromise between energy and intensity determination (equation (4)). These directions are not sufficient to guarantee the uniqueness of the interdimer coupling scheme. A conclusive extension of the experimental data is presented in section 4, tailored to particularly significant energy directions in reciprocal space. The second aim pursues the refinement of the microscopy behind the effective dimer parameters, as listed in table 1. At first order, different combinations of single-ion couplings in $H^{(1)}$ are easily shown to generate the same interdimer coupling. Between dimer i and dimer j the most general microscopic interaction involves four different and competing exchanges, according to the four possible spin–spin combinations. They all enter J_{ij} as a weighted average, following

$$J_{ij} = \frac{1}{2}(J_{ij,11} + J_{ij,22} - J_{ij,12} - J_{ij,21}) \tag{5}$$

in a notation already introduced. The first two contributions on the right-hand side of equation (5) correspond to a microscopic ladder-like coupling scheme; the last two contributions apply to a zigzag-like case [13, 14]. Their opposite signs are imposed by the relative phases of the single spins involved. In the case of competition between these interactions $J_{ij} \sim 0$, and the excitations remain localized [15]. Reflecting the spirit of the dimer approach, the information determined from the model parameters at leading order is insensitive to such single-ion correlations, but rather provides the effective dimer correlation. Only in a second-order expansion can the single-ion contributions in principle be isolated from the dispersion relation, according to

$$\begin{aligned}\epsilon_{\pm}^{(2)}(q) = &-\frac{1}{J}\{J_a^2 + J_{a2c}^2 + 2J_{abc}^2\} + \frac{1}{2J}\{\epsilon_{\pm}^{(1)}(q)\}^2 \\ &+ \frac{1}{J}\{F_a^2 + F_{a2c}^2 + 2F_{abc}^2 - G_a^2\cos(2\pi q_h) - G_{a2c}^2\cos(4\pi q_h + 2\pi q_l) \\ &\mp 2G_{abc}^2\cos(\pi q_k)\cos(2\pi q_h + \pi q_l)\}\end{aligned} \tag{6}$$

with

$$\begin{aligned}F_{ij}^2 &= \frac{1}{4}(J_{ij,11} - J_{ij,22})^2 + \frac{1}{4}(J_{ij,12} - J_{ij,21})^2 \\ G_{ij}^2 &= \frac{1}{4}(J_{ij,11} - J_{ij,22})^2 - \frac{1}{4}(J_{ij,12} - J_{ij,21})^2.\end{aligned} \tag{7}$$

$\epsilon_{\pm}^{(2)}(q)$ given above consists of a constant term and a higher Fourier term, both depending on the effective dimer couplings already introduced, plus a basic Fourier term containing the details of the single-ion couplings after equation (7). The notation refers to table 1, which provides the microscopic data corresponding to the proposed single-ion couplings. Although

Table 2. Values of the dimer exchange coupling constants for $KCuCl_3$ at $T \sim 2$ K. The parameters are fit results obtained using a model explained in the text, considering first-order (O(1), left) and second-order expressions (O(2), right). Errors correspond to one standard deviation; the calculated gap Δ is given in the bottom line.

J_{ij}	R_{ij} (l.u.)	O(1) (meV)	O(2) (meV)
J_a	$\pm(1\ 0\ 0)$	0.217(7)	0.210(5)
J_{a2c}	$\pm(2\ 0\ 1)$	0.382(8)	0.340(5)
J_{abc}	$\pm(1\ 1/2\ 1/2)$	−0.417(5)	−0.372(4)
	$\pm(1\ \bar{1}/2\ 1/2)$		
J	$(0\ 0\ 0)$	−4.273(6)	−4.287(4)
Δ		2.84(3)	2.72(2)

$KCuCl_3$ belongs to the limit where these single-ion corrections are severely subordinated to the dominant coupling J (table 2), we will show that the overall effect determined by $\epsilon_{\pm}^{(2)}(q)$ significantly improves the quality of the data analysis.

4. Measurements

Inelastic neutron scattering investigations were performed at fixed final energy $E_f = 4.7$ meV on the cold three-axis spectrometers IN14 (ILL, Grenoble) and DrüchaL (SINQ at PSI, Villigen), operated in the constant-κ mode under standard focusing conditions. Data were collected at $T \sim 2$ K in the a^*c^*- and b^*c^*-planes, respectively. With respect to the gap $\Delta = 31.1$ K (after [16]) the chosen temperature $T \ll \Delta$ ensures that the magnetic system is in its ground state. The energy determination at a given κ is the result of Gaussian fits to the observed profiles. Standard errors in their centre positions typically amount to less than a few 10^{-2} meV, and never exceed the symbol size adopted in the graphical representation of the dispersion relation (figures 2 and 3).

In figure 2, selected directions on the symmetry a^*c^*-plane are presented in a reduced scheme representation. Points measured in different zones have been arranged to build a continuous path in reciprocal space, according to the dimer lattice symmetry. Starting from the known dispersion relations along $(0, 0, x)$ and $(x, 0, 0)$ (panel I and III, respectively), new selected directions are introduced and evaluated at first order in the light of different interdimer coupling schemes (dotted, dashed–dotted and dashed curves) to be explained in the following. The scheme corresponding to equation (3) (dotted curve) is supplemented by the second-order corrections derived in equation (6) (continuous curve). As anticipated in section 2, this scheme will completely account for the experimental observations. However, from a dimer point of view, e.g. neglecting the microscopy of the exchange paths and considering the dimers as featureless magnetic units, there is no reason to prefer the strongly directional couplings of equation (3) with respect to other coupling combinations. As exemplified for the exchange path J_{a2c}, the following substitutions can be proposed:

$$J_{a2c}\cos(4\pi q_h + 2\pi q_l) \rightarrow J_{a2}\cos(4\pi q_h) + J_c\cos(2\pi q_l) \tag{8}$$

$$J_{a2c}\cos(4\pi q_h + 2\pi q_l) \rightarrow J'_{a2c}\cos(4\pi q_h + 2\pi q_l) + J'_{a2\bar{c}}\cos(4\pi q_h - 2\pi q_l) \tag{9}$$

where the right-hand side in equations (8) and (9) is meant to replace the appropriate Fourier term in equation (3), as indicated. The substitution scheme corresponding to equation (8) splits the original exchange path J_{a2c} into two separate exchange paths J_{a2}, J_c; the substitution scheme corresponding to equation (9) considers a symmetric extension J'_{a2c}, $J'_{a2\bar{c}}$: both are

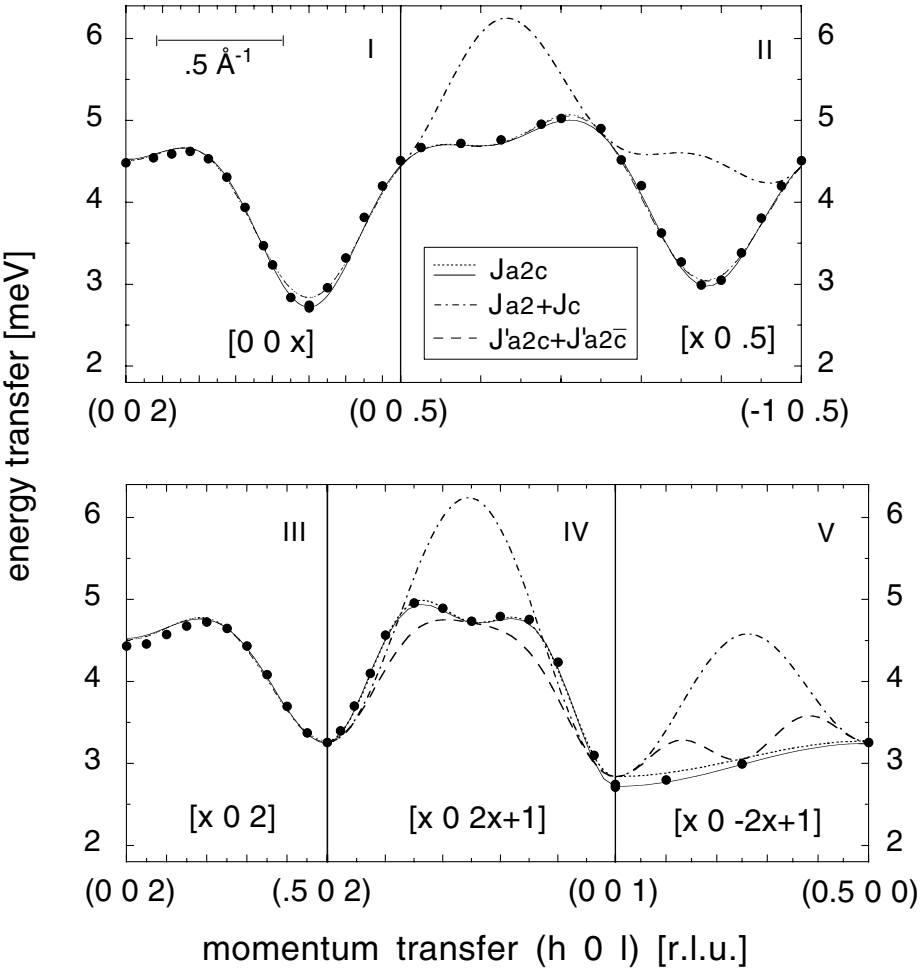

Figure 2. The measured energy dispersion (full points) of the magnetic excitations in the symmetry a^*c^*-plane of $KCuCl_3$ at $T \sim 2$ K. First-order perturbation calculations for different interdimer coupling schemes are shown as dotted, dashed–dotted and dashed lines, according to models described by equations (3), (8) and (9), respectively. Second-order corrections (continuous lines) refer to equation (6).

irrespective of the preferred planar orientation of the dimers in the unit cell, as discussed. Nevertheless, the fits resulting on imposing the conditions $J_{a2} = J_c$ and $J'_{a2c} = J'_{a2\bar{c}}$ in equations (8) and (9), respectively, are easily shown to account for the totality of the measurements presented in [6, 7]. This is due to the fact that only projections of the original J_{a2c}-coupling along the crystallographic axes enter the directions investigated, as illustrated in the present work for $(0, 0, x)$ and $(x, 0, 0)$ in panel I and panel III of figure 2. Obviously however, selected directions in reciprocal space allow one to uniquely determine the correct interdimer scheme. The new results along $(x, 0, 0.5)$ presented in panel II discard the scheme corresponding to equation (8) (dashed–dotted curve), which does not feature the correct modulation, but cannot discriminate between equation (3) (dotted curve) and equation (9) (dashed curve). To resolve this issue, scans along mixed directions are reported in panels IV and V: the scheme corresponding to equation (9) is found to be inappropriate to describe the

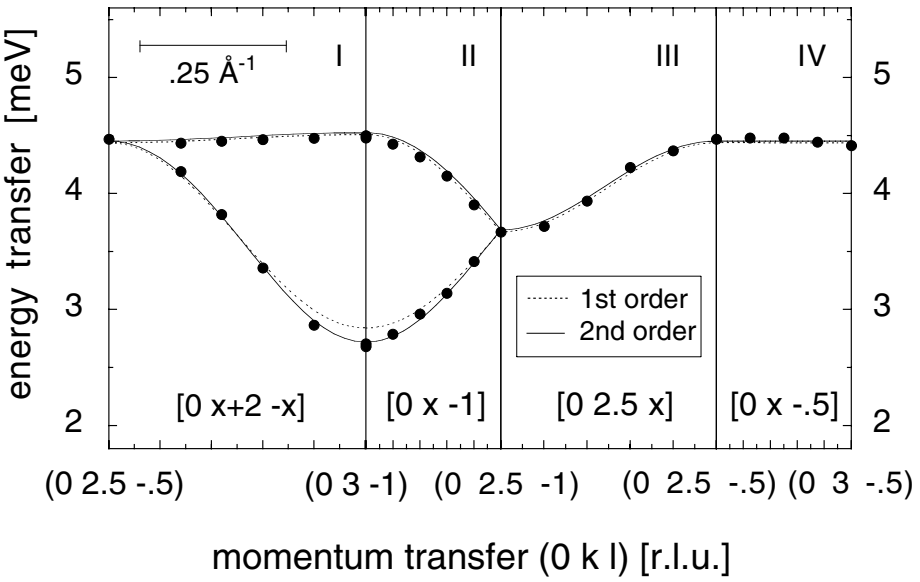

Figure 3. The measured energy dispersion (full points) of the magnetic excitations in the generic b^*c^*-plane of $KCuCl_3$ at $T \sim 2$ K. Lines correspond to fits to a first-order (dotted) and second-order (continuous) dimer perturbation model, as described by equations (3) and (6), respectively.

experimental observations, too. The points presented in panel V cover a direction perpendicular to both the J_{a2c}- and J_{abc}-couplings of equation (3), which as a result do not contribute to the dispersion. The observed modulation can only be caused by additional couplings, and is consistently explained by J_a as predicted from equation (3). The bandwidth of the dispersion along $(x, 0, -2x)$ is thus a direct measurement of $|2J_a|$. Investigations on both the a^*c^*- and b^*c^*-planes confirm the uniqueness of J_{abc}-coupling with respect to other coupling combinations, as well.

In the generic b^*c^*-plane (figure 3) two excitation branches are generally expected (panel I and II). Phase-coherent and antiphase-coherent excitations between edge and centre dimers both enter $S_{\pm}(\kappa, \omega)$ at once according to equation (4). Their energy difference depends on the couplings connecting the two sublattices, which after the scheme of equation (3) reduce to

$$|\epsilon_+(q) - \epsilon_-(q)| = |4J_{abc}\cos(\pi q_k)\cos(2\pi q_h + \pi q_l)|. \tag{10}$$

Following the peculiar q-dependence in the above expression, degeneracy of the two branches can be selectively imposed either for $q_k = \pm 0.5$ or for $(2q_h + q_l) = \pm 0.5$, modulo a reciprocal-lattice vector. Both features have been successfully tested in panels III and IV. For the particular set of points presented in panel IV, no dispersive behaviour is expected, since J_a and J_{a2c} are kept constant as well. We interpret the results presented in figure 2 and figure 3 as the conclusive verification at leading order of the effective coupling scheme derived in the previous section, and formalized in equation (3). Besides, this discussion demonstrates that the magnetic properties in $KCuCl_3$ are three-dimensional in nature because of the presence of three noncollinear interdimer couplings J_a, J_{a2c}, J_{abc} additional to the dominant intradimer coupling J. Considering the moderate J_a-contribution to the energy dispersion in panel V of figure 2, excitations delocalize, however, preferentially on the plane determined by the tilted arrangement of the dimers in the cell (figure 1), which involves the J_{a2c}- and J_{abc}-couplings.

The fitted model parameters from equation (3) including second-order corrections from

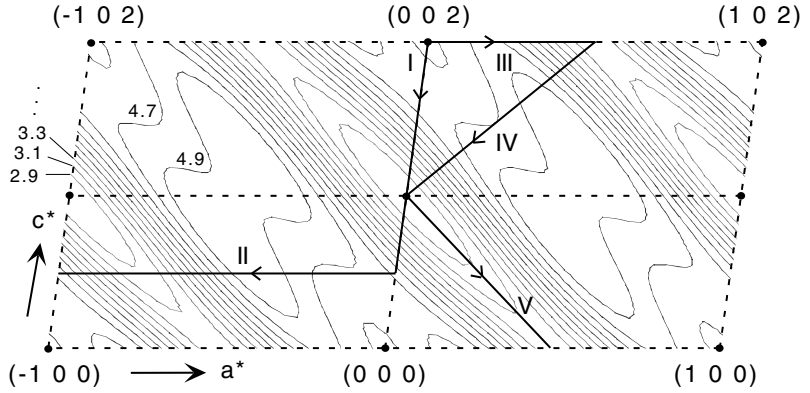

Figure 4. The calculated energy dispersion of the magnetic excitations in the symmetry a^*c^*-plane of $KCuCl_3$ at $T \sim 2$ K; cf. equations (3) and (4). Minima correspond to $q = (0, 0, \pm 1)$ (r.l.u.), with a period $\tau = (1, 0, 0)$ along $\boldsymbol{a}^*$ and $\tau = (0, 0, 2)$ along $\boldsymbol{c}^*$. Contour lines separate 0.2 meV energy steps; straight lines refer to the reduced paths shown in figure 2 (panels I–V).

equation (6) are reported in table 2. The AF intradimer coupling $J \sim -4.3$ meV is one order of magnitude bigger than the interdimer couplings, largely fulfilling the validity criteria of the model approach. Its strength corresponds to ∼50 K in good agreement with a dimer quantum Monte Carlo analysis of the susceptibility χ over the whole temperature range [8], yielding $|J| = 49.2$ K as best fit. The weak interdimer couplings in $KCuCl_3$ give rise to appreciable bandwidth because of their additive contributions to the dispersion relation. After equations (3) and (4), effective phase correlations are interpreted as ferromagnetic between dimers belonging to the same sublattice ($J_a > 0$, $J_{a2c} > 0$), and antiferromagnetic between dimers of different sublattices ($J_{abc} < 0$). In the symmetry a^*c^*-plane, minima are observed at $q = \pm(0, 0, 1)$ and magnetic equivalent points $\kappa = q+\tau$, which are obtained by translation τ along $\boldsymbol{a}^*$ or along $2\boldsymbol{c}^*$ (figure 4). The quantitative determination of the coupling constants favourably compares with previous RPA results, with overall discrepancies in the numerical values smaller than 0.1 meV or ∼2% on the scale of $|J|$. The effect of the second-order expansions clearly improves the quality of the model description, in particular around the minima of the dispersion relation (continuous lines in figure 2, figure 3). A very weak additional effective coupling reported in [7] is likely to originate from such higher-order corrections, and has not been included in the present starting coupling set (table 1).

Different selected single-ion exchange configurations have been considered in the second-order refinement procedure. The microscopic parameters from figure 2, figure 3 and table 2 correspond to the following couplings: $J_{a2c,12}$ $(=-2J_{a2c})$, $J_{abc,11} = J_{abc,22}$ $(=2J_{abc})$, $J_{a,11} = J_{a,22}$ $(=J_a)$, which are illustrated in figure 1. Values in brackets reproduce the effective dimer couplings resulting from the given single-ion couplings, and are reported in table 2. The gap calculated from the minimum of the dispersion relation $\epsilon^{(0)} + \epsilon^{(1)} + \epsilon^{(2)}$ corresponds to $\Delta = 2.72(2)$ meV ~ 32 K, in excellent agreement with high-field magnetization results [16].

5. Conclusions

We presented a complete neutron investigation of the Cu^{2+} $S = 1/2$ compound $KCuCl_3$. This unconventional magnetic insulator has a singlet ground state and shows gapped triplet excitation modes of dimer origin. The nature of the observed excitations is three dimensional in q-space, despite the lack of magnetic order in the ground state. This is explained by a

severe imbalance in the strength of the exchange constants involved. Within the framework of a dimer AF Heisenberg model, the dispersion relation of the excitations above the gap has been successfully compared to detailed model predictions. Attention has been paid to providing microscopic support to the effective model parameters. Since the unconventional magnetic interactions in $KCuCl_3$ are directly related to the low crystal symmetry, the exchange constants have been critically discussed considering the structural coordination of the Cu^{2+} ions in the unit cell. In accordance with earlier investigations, $KCuCl_3$ is interpreted as an isotropic antiferromagnetic dimer compound, featuring weak interdimer couplings additionally to a dominant intradimer coupling $J \sim -4.3$ meV. The latter connects spin pairs along the rungs of the double chains to build nearly planar Cu_2Cl_6 dimers. The relative orientation of the dimers in the cell is such as to favour $(2x, 0, x)$ and $(x, \pm x/2, x/2)$ superexchange pathways. An $(x, 0, 0)$ exchange completes the effective coupling scheme within the model approach derived in the text. The observed excitations confirm the validity of the above dimer scheme and support, at leading order, its uniqueness within experimental accuracy. The single-ion contributions to the effective dimer couplings considered have been generally presented in terms of second-order expectations. The interactions discussed possibly apply to the parent quantum systems $TlCuCl_3$ and NH_4CuCl_3 as well [17], albeit at different coupling strength ratios. In the light of the comprehensive experimental characterization of the title compound, a comparison with *ab initio* LDA calculations would be very interesting.

Acknowledgments

It is a pleasure to thank B Braun, K Kakurai, H J Mikeska, B Normand and M Troyer for stimulating discussions. Financial support given by the Swiss National Science Foundation is gratefully acknowledged.

References

[1] Cowley R A, Lake B and Tennant D A 1996 *J. Phys.: Condens. Matter* **8** L179
[2] Garrett A W, Nagler S E, Tennant D A, Sales B C and Barnes T 1997 *Phys. Rev. Lett.* **79** 745
[3] Willett R D, Dwiggins C, Kruh R F and Rundle R E 1963 *J. Chem. Phys.* **38** 2429
[4] Thornley J H M, Mangum B W, Griffiths J H E and Owe J 1961 *Proc. Phys. Soc.* **78** 1263
[5] Bencini A and Gatteschi D 1990 *EPR of Exchange Coupled Systems* (Berlin: Springer)
[6] Kato T, Takatsu K, Tanaka H, Shiramura W, Mori M, Nakajima K and Kakurai K 1998 *J. Phys. Soc. Japan* **67** 752
[7] Cavadini N, Henggeler W, Furrer A, Güdel H U, Krämer K and Mutka H 1999 *Eur. Phys. J.* B **7** 519
Cavadini N, Henggeler W, Furrer A, Güdel H U, Krämer K and Mutka H 2000 *Physica* B **276–278** 540
[8] Nakamura T and Okamoto K 1998 *Phys. Rev.* B **58** 2411
[9] Rice T M, Gopalan S and Sigrist M 1993 *Europhys. Lett.* **23** 445
Müller T F A, Anisimov A, Rice T M, Dasgupta I and Saha-Dasgupta T 1998 *Phys. Rev.* B **57** R12 655
[10] Kato T, Oosawa A, Takatsu K, Tanaka H, Shiramura W, Nakajima K and Kakurai K 1999 *J. Phys. Chem. Solids* **60** 1125
[11] Damle K and Sachdev S 1998 *Phys. Rev.* B **57** 8307
[12] Barnes T, Riera J and Tennant D A 1999 *Phys. Rev.* B **59** 11 384
[13] Normand B, Penc K, Albrecht M and Mila F 1997 *Phys. Rev.* B **56** R5736
[14] Kolezhuk A K and Mikeska H J 1997 *Phys. Rev.* B **56** R11 380
[15] Miyahara S and Ueda K 1999 *Phys. Rev. Lett.* **82** 3701
[16] Shiramura W, Takatsu K, Tanaka H, Kamishima K, Takahashi M, Mitamura H and Goto T 1997 *J. Phys. Soc. Japan* **66** 1900
[17] Tanaka H, Shiramura W, Takatsu T, Kurniawan B, Takahashi M, Kamishima K, Takizawa K, Mitamura H and Goto T 1998 *Physica* B **246–247** 230